Journal of Hydrology 617 (2023) 129087

Contents lists available at ScienceDirect

Journal of Hydrology

journal homepage: www.elsevier.com/locate/jhydrol

Research papers

Ecohydrological metrics derived from multispectral images to characterize surface water in an intermittent river

Thiaggo C. Tayer [a,b,*], Leah S. Beesley [a,b], Michael M. Douglas [a,b], Sarah A. Bourke [c], J. Nik Callow [a,b], Karina Meredith [d], Don McFarlane [a]

[a] School of Agriculture and Environment, The University of Western Australia, Stirling Highway, Crawley, WA 6009, Australia
[b] Northern Australia Environmental Resources Hub, National Environmental Science Program, Brisbane, Queensland, Australia
[c] School of Earth Sciences and National Centre for Groundwater Research and Training, University of Western Australia, Crawley, WA 6009, Australia
[d] Australian Nuclear Science and Technology Organisation, Institute for Environmental Research, Lucas Heights, NSW 2232, Australia

ARTICLE INFO

Keywords:
Hydrological metrics
Remote sensing
River management
Ecohydrology
Intermittent rivers
Northern Australia

ABSTRACT

Accurately describing the hydrology of intermittent rivers is a critical step in improving our understanding and management of freshwater ecosystems. Traditional approaches such as using gauged discharge data provide little information once flow ceases and no insight into the location, morphology, or persistence of river pools. However, multispectral images can be used to describe surface water, characterize hydrology, and provide insight into ecological functioning. A multispectral approach is highly cost-effective and well suited to remote intermittent rivers with little or no gauging infrastructure. Here, we develop an algorithm to extract hydrological attributes (i.e., pool area, length, perimeter, and mean width) from multispectral imagery (Sentinel-2) and use these attributes to create a suite of ecologically relevant hydrological metrics. We describe changes in attributes and metrics in a large lowland intermittent river as it transitions from wet to dry over a four-year period. We also describe temporal changes in attributes and metrics among five river sections with contrasting hydrological persistence and fragmentation. Our algorithm successfully identified surface water in the main channel and the adjacent floodplain, the centerline of pools, and their upstream and downstream ends. Metrics proved effective at describing seasonal patterns in hydrology; revealing how the size, complexity, and elongation of surface water features (e.g., pools) decreased as the study river transitioned from wet to dry and how fragmentation increased. Metrics also successfully differentiated the river sections with varied hydrological persistence. Ecohydrological metrics derived from multispectral imagery have the potential to provide meaningful insights into riverine morphology, resilience, and ecological functioning. Our spatial approach represents a significant advancement in the ability to characterize and manage intermittent rivers, which are increasingly threatened by water resource development and a drying climate.

1. Introduction

Intermittent streams and rivers, characterized by periods of no-flow, account for at least half of the length of all the world's rivers (Datry et al., 2017; Messager et al., 2021). They are becoming increasingly widespread due to water resource development and climate change in regions with drier climate trends (Smettem et al., 2013). Intermittent rivers sustain unique biodiversity and provide a range of goods and services that people depend on (Acuña et al., 2014; Boulton, 2014; Datry et al., 2014). In recognition of their importance, and the threats they face, intermittent rivers are receiving greater attention (Blackman et al., 2021; Chiu et al., 2017; Datry et al., 2017; Koundouri et al., 2017; Larkin et al., 2020), even though they have been historically under-represented in the hydrologic literature (Shanafield et al., 2021).

Accurately describing the hydrology of intermittent rivers is a critical step in improving our understanding and management of these systems, as it allows us to characterize their natural state, assess impacts, and monitor recovery; however, describing the hydrology of intermittent rivers is often not straightforward. Traditional approaches such as using gauged discharge data provide little information once flow ceases and no insight into the location, morphology, or resilience of river pools. Moreover, this type of approach is costly, as it requires field

* Corresponding author at: School of Agriculture and Environment, The University of Western Australia, Stirling Highway, Crawley, WA 6009, Australia.
E-mail address: tayerthiaggo@gmail.com (T.C. Tayer).

https://doi.org/10.1016/j.jhydrol.2023.129087
Received 1 August 2022; Received in revised form 27 December 2022; Accepted 5 January 2023
Available online 7 January 2023

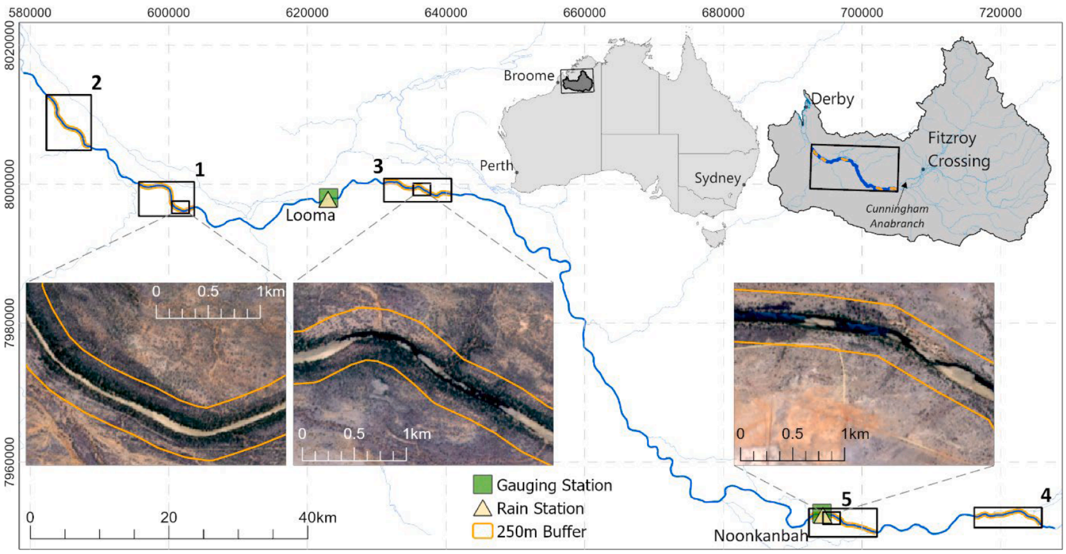

Fig. 1. Location of the study area in the Fitzroy River, Western Australia. The numbers above each location box (i.e., 1,2,3,4,5) represent the broad river section classification, where 1 was the least persistent and 5 the most. The inset boxes showing satellite imagery show an example of the water persistence gradient in some of the studied sections (1, 3 and 5) at the end of the dry season of a particularly dry year (October – 2019). The orange lines represent the 250 m buffer. (For interpretation of the references to colour in this figure legend, the reader is referred to the web version of this article.)

maintenance. Consequently, many large rivers in remote and dryland regions have sparse or no hydrological gauging data (Callow and Boggs, 2013). Hydrologic and hydrodynamic models generated from Digital Elevation Models (DEMs) are an alternative method to characterize flood extent and other river characteristics, but they also have limitations. For instance, hydrologic and hydrodynamic models are dependent on DEM spatial resolution and are particularly sensitive to DEM accuracy in dryland landscapes (Callow et al., 2007; Callow and Smettem, 2009). Highly accurate DEMs are also rarely available in remote dryland river basins due to the high costs of producing them, also they often need extra correction and processing steps to better represent the known hydrology (Jarihani et al., 2015). Despite these limitations, gauged discharge data or hydrologic models are still the primary means for the ecohydrological characterization and classification of rivers, including intermittent rivers (Bond and Kennard, 2017; D'Ambrosio et al., 2017; Kennard et al., 2010; Olden et al., 2012; Richter et al., 1996).

Multispectral imagery can provide a different perspective on the hydrology of intermittent rivers and has the potential to overcome some of the limitations of gauging data or hydrologic models due to their high frequency, temporal and spatial continuity, and lower costs. Multispectral images can be analyzed to generate attributes for surface water (e.g., pool area, length, perimeter) along the length of a river, or for specific sections within a river, which can then be used to derive metrics (e.g., pool complexity, pool size) that provide insight into ecological functioning. While this is yet to be done in intermittent rivers, metrics derived from this type of imagery have been used in terrestrial environments to quantify landscape structure and change (Crowley and Cardille, 2020; Hermosilla et al., 2019; McGarigal and Marks, 1995; Olariu et al., 2022) and to describe the morphology of catchments (Beven et al., 1988; Frasson et al., 2019). Some of these metrics have the potential to be adapted and transferred to intermittent river systems to better understand their ecohydrological characteristics. For instance, metrics based on the size and shape of surface water features could be used to describe the amount and location of macro (e.g., main channel, floodplain) and mesohabitats (pool, runs, riffles). They can also provide an insight into the littoral zone extent, a zone with important ecological importance (Roach et al., 2014; Winfield, 2004; Yuan et al., 2013). Metrics based on morphology could also provide an insight into sedimentation, erosion, and infiltration rates (Gitz et al., 2015; Reddy et al., 2004), and those based on the persistence of surface water through time could be used to identify ecological refuge locations and provide insights into surface water and groundwater dynamics (Sims et al., 2016). Lastly, metrics based on surface water connectivity could provide an insight into the downstream transport of physical and biological particles, river fragmentation and the potential for organism dispersal (Pringle, 2010; Pringle, 2001; Ward et al., 2002). Thus, ecohydrological metrics derived from multispectral images offer much promise as a cost-effective way to generate information that can support the management and protection of intermittent river systems.

The broad aim of this study was to generate novel hydrological metrics derived from multispectral imagery, obtained from Sentinel-2A and −2B satellites that have the potential to provide an insight into the ecology of intermittent rivers. We had four specific aims: 1) develop an algorithm to extract hydrological attributes (e.g., area, length, perimeter, and mean width) about surface water from multispectral imagery; 2) use these attributes to create a suite of ecologically-relevant hydrological metrics; 3) describe changes in attributes and metrics in a river system as it transitioned from wet to dry; and 4) describe seasonal variation in each attribute and metric within river sections with contrasting hydrological persistence and fragmentation. Characterizing intermittent rivers using this approach can support the management and protection of semi-arid environments facing increasing pressures from development and climate change and provide an insight into the benefits of an optical remotely sensed approach compared to conventional gauged discharge data.

2. Materials and methods

2.1. Study area and design

The study was undertaken in the Fitzroy River, located in the semi-arid Kimberley region of Western Australia (Fig. 1). It has a catchment area of approximately 94,000 km^2 and a length of 733 km (Harrington et al., 2011; Petheram et al., 2018). The Fitzroy catchment exhibits distinct hydrological seasonality, experiencing extreme flood flows during wet times of the year (November–April), with 87 % of the runoff occurring between January and March before drying to loosely interconnected pools in the dry period (May-October) (Beesley et al., 2021; Charles et al., 2016; Petheram et al., 2018). There is extreme spatial and temporal variation in water extent, with the maintenance of hydrological connectivity constrained by the strong seasonal climate variation and the influence of groundwater discharge zones (Taylor et al., 2018). The water sustaining persistent pools comes either from groundwater discharging from the local alluvial aquifers associated with the river's floodplain, or the regional groundwater associated with sedimentary sandstones of the Grant Group and Poole Sandstone (Harrington et al., 2011; Harrington and Harrington, 2015; Taylor et al., 2018). Rainfall in a hydrological year (Nov-Oct) is highly variable. For instance, in the last three hydrological years (2019–2021), the catchment experienced the lowest (348 mm – 2019) and second-highest total rainfall (854 mm – 2021) measured over the last 19 years (2003–2022) for the average of the two closest rain stations Noonkanbah and Looma (Fig. 1). This variable rainfall manifest in highly divergent stream discharge over the study period for two gauging stations – Noonkanbah and Looma (Department of Water and Environmental Regulations Water Information Reporting system).

The main channel of the Fitzroy River was visually defined and manually vectorized using ArcGIS Pro 3.0 and Esri base maps. The area of interest was defined as a 250 m wide buffer on each side of the manually vectorized drainage line. Five river sections were chosen along the lowland stretch of the river, between the confluence with the Cunningham Anabranch to approximately 100 km upstream of the estuary (Fig. 1). We chose to perform our study on five representative sections rather than the entire river to make our study more tractable. Our five focal sections had approximately the same surface area (5.1 km^2) and spanned the same length of the main channel river (10.2 km). Our focal sections spanned a hydrological continuum from persistent (high likelihood of groundwater discharge) reaches to intermittent (low likelihood of groundwater discharge) reaches, allowing us to evaluate the ability of our metrics to differentiate a hydrological persistence gradient. The 10.2 km length was somewhat arbitrarily chosen, but we considered it suitable for our aim as it was large enough to confidently characterize a river section's hydrology but was not so large that it spanned regions with very different water persistence conditions. River sections were broadly classified as:

1. low persistence, very fragmented with very little or no water at the end of the dry season;
2. low persistence, very fragmented with some water at the end of the dry season;
3. intermediate persistence, fragmented, but with refuge pools containing water at the end of the dry season;
4. high persistence, low fragmentation, with refuge pools and a considerable extent of water at the end of the dry season; and,
5. very high persistence, low fragmentation, with a considerable extent of refuge pools and water at the end of the dry season.

Our classification was based on a thorough visual inspection of fortnightly remotely sensed multispectral imagery (Sentinel-2) captured in a particularly dry year (2019), a long-term study of pool persistence using Landsat (Sims et al., 2016), and knowledge of the hydrology of the river as reported by Harrington et al., (2011), Harrington and Harrington (2016), Harrington and Harrington (2015), Sims et al., (2016) and Taylor et al., (2018).

2.2. Image datasets

Sentinel-2 multispectral surface reflectance NBART images (Nadir BRDF Adjusted Reflectance + Terrain Illumination Correction) downloaded from the Digital Earth Australia (DEA) database (http://www.ga.gov.au/dea (accessed on 15th October 2022)) through the National Computational Infrastructure (NCI), reprojected to UTM/WGS84, were used in this study. Geoscience Australia used several pre-processing techniques for Sentinel-2 (Li et al., 2012, 2010; Vincenty, 1975); a detailed description can be found at: https://cmi.ga.gov.au/data-products/dea/190/dea-surface-reflectance-nbart-sentinel-2-msi#basics. We used all available images (5-day return) from 01 to 12-2017 to 30–11-2021, selecting those with at least 40 % of valid pixels (i.e., maximum of 60 % of cloud/shadow cover) within a 1 km buffer distance on each side of the main channel drainage line.

2.3. Defining and deriving metrics extracted from multispectral imagery to characterize intermittent rivers

2.3.1. Method workflow

The study workflow was divided into three parts: extracting attributes, deriving metrics, and describing and evaluating attributes and derived metrics. The first part extracted hydrological attributes at pool level from multispectral imagery in sixteen steps (Fig. 2 and Fig. 3). The second part used the extracted attributes to calculate the developed metrics (Section 2.3.4) for the focal river sections. The third part described and evaluated hydrological attributes and derived metrics changes as the river system transitioned from wet to dry seasons (Section 2.3.5).

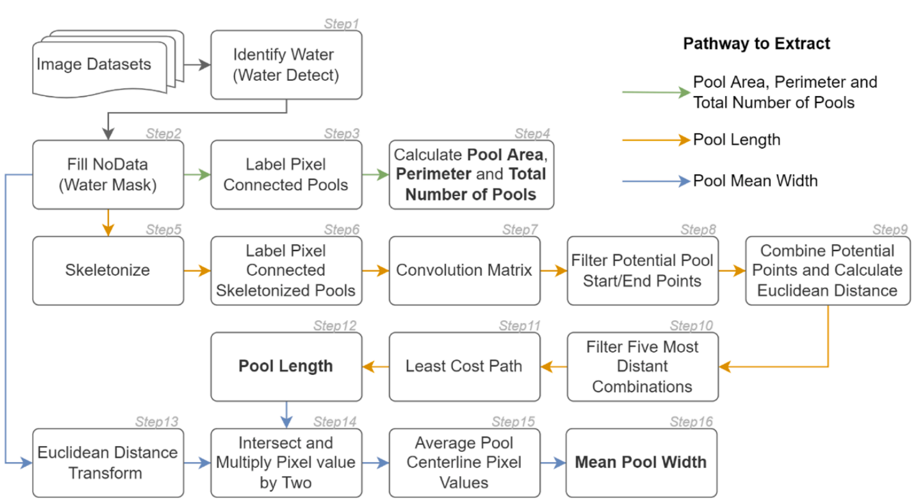

Fig. 2. Processing workflow for extracting hydrological attributes from multispectral images. Attributes are shown in bold letters. Distinct colored arrows represent three different pathways to extract the five hydrological attributes (i.e., Pool Area, Perimeter, Length, Mean Width, and Total Number of Pools).

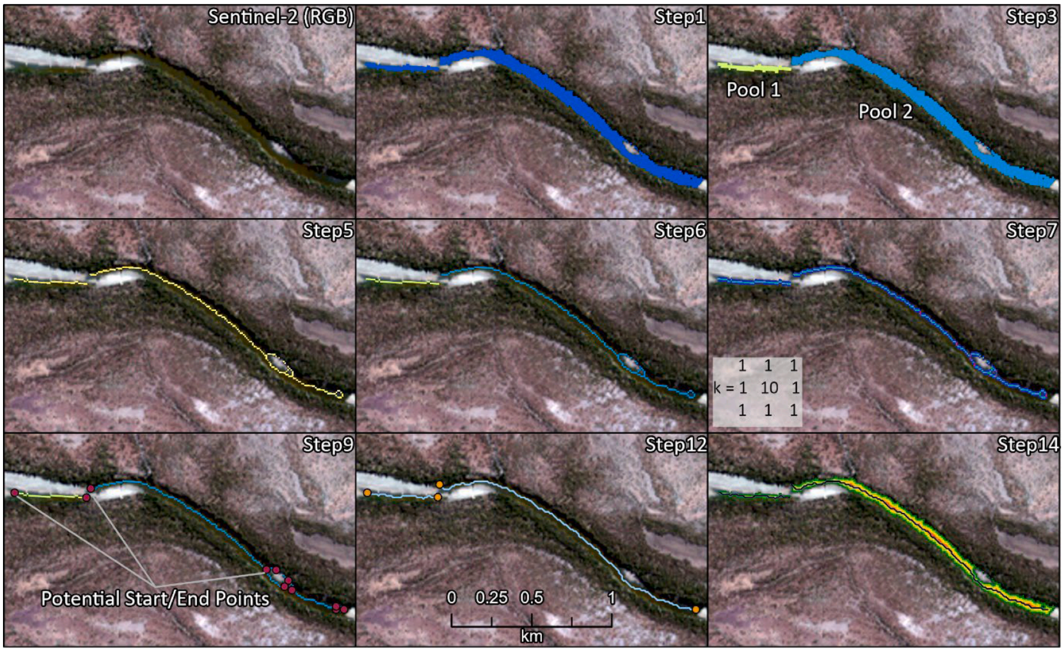

Fig. 3. Visual examples of a section of the river and a subset of the steps taken for extracting hydrological attributes with Sentinel-2 RGB (Red, Green and Blue bands) composition in the background. Panels show important processes such as water identification (Step 1 – water in blue); pools being differentiated (Step 3 – different pools in blue and light green); a skeletonized representation of the water mask (Step 5), and the differentiation of skeletonized pools (Step 6); the convolution filtering using a custom kernel (k) (Step 7); calculation of Euclidean distances for the combination of potential pool Start and end points represented by red dots (Step 9); the longest least cost path (pool length) represented by a light blue line and the final pool start/end points as orange dots (Step 12); and the Euclidean distance transform represented by a range of colors going from green to red, where red represents the furthest and green the closest points from the pool nearest border (Step 14). The location of each step inside the workflow is shown in Fig. 2. (For interpretation of the references to colour in this figure legend, the reader is referred to the web version of this article.)

2.3.2. Identifying water

A preliminary step prior to metric generation was to map surface water extent (Step 1). This was done using the Water Detect algorithm (Cordeiro et al., 2021) with Sentinel-2 images (10 m – B: Blue, G: Green, R: Red, NIR: Near-infrared) and adopting the input parameter values proposed for this catchment by Tayer et al. (2023) (i.e., maximum clustering: 6; regularization: 0.07). The Water Detect algorithm was executed for every image (see Section 2.2), and the results were clipped to the area of interest (250 m buffer on each side of the drainage line). The output of Water Detect is a binary array with values of one for water pixels and zero for non-water pixels; minus one represents ‘no data’ values. As the focus of this paper was to capture seasonal patterns, especially the contraction of surface water during the dry season, the clipped water mask time series was concatenated and reduced into two composites per month (~15-day composites) in a single Data Array (Dask Development Team, 2016; Hoyer and Hamman, 2017), where the maximum pixel value was taken for conflicting values (i.e., overlapping values within a composite). Of the resulting 112 composite images, only two had cloud coverage above 60 %, and 88 composites were below 5 %.

The water mask binary array was checked for missing values in each layer of the time series since ’no data’ values, such as cloud and shadow masks, can influence water extent estimation, falsely breaking river connectivity and causing potential misinterpretation of parameter values. The missing values were populated using the following conditions (Step 2): a) The ’no data’ value was filled with the first next valid observation or the second if the next immediate value was also missing (i.e., backward fill); b) if the value was in the last position of the time series, or c) if the backward filling was unable to fill missing values, we used a forward fill propagating up to two observations before the missing value. If none of these conditions were satisfied, the missing value remained unchanged as ’no data’.

2.3.3. Extracting hydrological attributes

After successfully mapping surface water features and addressing missing values for the entire time series, we extracted attributes of interest (i.e., pool area, pool length, pool mean width, pool perimeter, and number of pools) to be used as input variables for the proposed metrics. Here, we use the term ’pool’ to refer to a continuous area of surface water; thus, it may represent a range of geomorphic features, including pools, runs, glides, and riffles.

At each layer, pixel-connected regions were aggregated into unique groups using the Scikit-image morphology module ’Label’ function (van der Walt et al., 2014) (Step 3). This tool considers that two pixels are connected when they have the same value and are neighbors in any direction (lateral, vertical, or diagonal) (van der Walt et al., 2014); hence, each central pixel can potentially be connected with a maximum of eight neighboring pixels. After labeling connected regions, the attributes ’pool area’, ’pool perimeter’ and ’number of pools’ were retrieved for each unique group (i.e., pool) using Rasterio’s feature shape tool, where the number of pools corresponded to the total number of unique groups (Step 4).

To extract pool length, we first applied the Scikit-image morphology module ’Skeletonize’ function (Step 5), which reduces a binary image (e.g., water/non-water) to one-pixel wide representations (Lee et al., 1994). The resulting image is presented in the most simplified way without breaking connectivity and shape, in our case, representing the river centerline (or streamline) for each pool. However, the skeletonized output is not always represented by a unique line and can produce features with several connected nodes. To confine the skeletonized feature to the longest segment possible (i.e., pool length), we applied the Scikit-image measure module ’Label’ function to the skeletonized image, meaning that each connected river centerline segment was given a unique identifier (Step 6). We then proceeded to find the start and endpoints, or the most distant points, for each centerline. We used OpenCV’s (Bradski, 2000) built-in filter2D convolution function to apply a custom matrix (Kernel – k) to the skeletonized image (Step 7). Convolution filtering is a common technique for altering an image based on pixel neighbors adding each element to its local neighbors, weighted by a kernel. Examples of convolution filtering include smoothing, sharpening, blurring, and edge detection. Here, we used the following 3x3 custom kernel:

$$k = \begin{bmatrix} 1 & 1 & 1 \\ 1 & 10 & 1 \\ 1 & 1 & 1 \end{bmatrix}$$

Considering that we applied the kernel (k) to a binary water mask (water = 1 and non-water = 0), the maximum possible value of a pixel after the convolution is 18 if a water pixel is surrounded by eight other water pixels. The minimum is zero if a non-water pixel is surrounded by eight non-water pixels. We observed the most common cases for start and endpoints pixels in the skeletonized image with a water pixel had one or three neighboring water pixels, hence, with a pixel value after convolution of 11 or 13, respectively (Step 8). With each unique pool's potential start/endpoints, we calculated all possible combinations of start and endpoint and the Euclidean distance between these pairs of points (Step 9). We then selected the most distant five pairs to calculate the distance between each pair using the river centerline as the path (Step 10). We used the Scikit-image graph module 'MPC Geometric', which finds the least-cost path from two points through a given cost array (van der Walt et al., 2014) (Step 11). To ensure that the river path (i.e., skeletonized water pixels) was the only possible path between each start/endpoint, we set all non-water pixels to −1 (no data), keeping the analysis within the skeletonized pixels. The most distant path between the selected start/endpoint pairs was selected as the final segment (i.e., pool length) (Step 12).

Mean pool width was estimated using SciPy's Euclidean Distance Transform tool (Virtanen et al., 2020) with the water mask as input (Step 13). The tool receives as input a binary image and outputs a distance array, i.e., an array with the same dimensions as the input image, but where each pixel contains the Euclidean distance to the closest border (non-water) pixel. We intersected the pool length segment (Step 12) with the distance array to extract the distance values from the pool centerline to the nearest border and multiplied these values by two to cover both sides of the river or the total wetted width from each centerline pixel (Step 14). Finally, for each unique pool, we averaged the centerline pixel values (Step 15) to calculate the mean pool width (Step 16).

The hydrological attributes extraction process was automated (see Data Availability Statement), and the results of some attributes, such as pool area and perimeter, were compared to the values calculated in ArcGIS using the Calculate Geometry tool. We also performed a qualitative analysis for pool endpoints and length by exploratory visual interpretation.

2.3.4. Defining and deriving ecohydrological metrics

Using the extracted attributes above, we derived 11 ecohydrological metrics to describe river characteristics and assess differences between river sections. The metrics were separated into two distinct categories that reflect surface water morphology (Table 1) and hydrological resilience (Table 2). The resulting extracted attributes (i.e., pool area, pool perimeter, pool length, mean pool width, and number of pools) from Section 2.3.2 were used as inputs to derive the developed metrics. The source line of code for the time series water identification, attribute extraction and metrics calculation is available on GitHub for community editing and improvement via collaboration (see Data Availability Statement).

Morphological metrics quantitatively described pool shape (i.e., geometry) and size and were represented by five metrics: the Area-weighted Mean Shape Index, Area-weighted Elongation Ratio, Area-weighted Mean Pool Area, Area-weighted Mean Pool Length, and Area-weighted Mean Pool Width. All metrics were weighted by area, effectively meaning that large pools within a river section exerted more influence on the metric than small pools.

Table 1
Remotely sensed ecohydrological metrics that pertain to morphology, the formulas used to calculate them, their definition and a brief description of their ecohydrological relevance.

Metric name	Metric Equation	Unit	Definition	Ecohydrological Relevance
Area-weighted[#] Mean Shape Index[1]	$AWMSI = \sum_{i=1}^{n}\left[\left(\frac{0.25\times p_i}{\sqrt{a_i}}\right)\left(\frac{a_i}{\sum_{i=1}^{n}a_i}\right)\right]$	None*	Reflects the complexity of a geometric shape increasing as the shape becomes more irregular, i.e., more complex shapes have a longer perimeter for a given area.	• High shape index values (more complex) can negatively correlate with sediment accumulation (Gitz et al., 2015). • More complex shapes can indicate a more rugged topography. • May describe the extent of littoral aquatic habitat, which can be important for biogeochemical processes, macrophytes, small-bodied fish (Winfield, 2004; Yuan et al., 2013), and the zone of highest algal production in dryland rivers (Bunn et al., 2006).
Area-weighted Elongation Ratio[2]	$AWRe = \sum_{i=1}^{n}\left[\left(2\frac{\sqrt{a_i/\pi}}{l_i}\right)\left(\frac{a_i}{\sum_{i=1}^{n}a_i}\right)\right]$	None*	Represents the elongation of a geometric shape. More elongated shapes will have lower elongation ratios with longer lengths for a given area. Values are constrained between 0 and 1, where higher values represent more circular features and lower values, more elongated.	• May provide insight into sedimentation, infiltration and runoff rates. • Lower elongation ratio values (more elongated) tend to have a higher susceptibility to erosion and sediment load, whereas higher values (more circular) show higher infiltration and lower runoff (Reddy et al., 2004). • More sediment and lower runoff can lead to higher turbidity, impacting river productivity (Roach et al., 2014).
Area-weighted Mean Pool Area	$AWMPA = \frac{\sum_{i=1}^{n}a_i\times a_i}{\sum_{i=1}^{n}a_i}$	km^2	Describes the weighted average area of pools within a section.	• Can be used to describe the amount and location of macrohabitats (e.g., main channel, floodplain, tributary, estuary) and mesohabitats (pools, riffles/runs) that support different species and fulfill different ecological functions. • Pool size can provide an early indication of resilience, as it may be associated with both breadth of habitat and persistence during dry conditions (Pollino et al., 2018).
Area-weighted Mean Pool Length	$AWMPL = \frac{\sum_{i=1}^{n}l_i\times a_i}{\sum_{i=1}^{n}a_i}$	km	Describes the weighted average length of pools within a section.	
Area-weighted Mean Pool Width	$AWMPW = \frac{\sum_{i=1}^{n}w_i\times a_i}{\sum_{i=1}^{n}a_i}$	km	Describes the weighted average width of pools within a section.	

Notation – $i = 1,\ldots, n$ *pool*/p_i = perimeter of pool i/a_i = area of pool i/l_i = length of pool i/w_i = mean width of pool i/*dimensionless.
Adapted from [1]McGarigal and Marks (1995), [2]Schumm (1956).
[#]Area-weighted means that pools with a larger size exert greater influence than smaller pools.

Table 2
Remotely sensed ecohydrological metrics that pertain to resilience, the formulas used to calculate them, their definition and a brief description of their ecohydrological relevance.

Metric name	Metric Equation	Unit	Definition	Ecohydrological Relevance
Pixel Persistence	$PP = \frac{WP}{T} \times 100$	%	Represents the water persistence of each pixel through time as a percentage. Higher values indicate higher persistence.	• Allows water persistence to be quantified and supports the identification of refuge locations, which are essential for preserving biodiversity during dry periods.
Refuge Area	$RA = PP > 90\%{*}pixelarea$	km^2	Quantifies the total area extent of the most persistent water pixels by counting the pixels with persistence values above 90 % and multiplying by pixel area.	• Can provide insight into hydrological dynamics because the distribution and extent of persistent water features at a large scale can reveal hydrological connectivity to groundwater, and at a small scale can reveal hyporheic interactions (Sims et al., 2016). • Sections with high pixel persistence indicate locations with either deep water or sufficient groundwater contribution to offset losses, also revealing refuge areas.
Wetted Area Percentage of Section[1]	$APSEC = \frac{\sum_{i=1}^{n} a_i}{sa} \times 100$	%	Describes how persistent the wetted extent is in relation to the section area. Calculated by dividing the section water extent (sum of pool areas within a section) by the total area of the section. APSEC approaches zero when water extent becomes increasingly rare in the landscape and indicates the severity of aquatic habitat contraction within a section.	• Indicates how severely aquatic habitat contracts or floods within a section and is also relevant to section-scale water persistence.
Wetted Length Percentage of Section[1]	$LPSEC = \frac{\sum_{i=1}^{n} l_i}{sl} \times 100$	%	Represents the ratio between the sum of pool length within a section and section wetted length. Considers the main channel drainage line within a river section as a reference (i.e., section wetted length). Values approaches zero as total pool length diminishes within a section.	
Pool Fragmentation	$PF = \frac{N}{\sum_{i=1}^{n} a_i}$	Pool/ km^2	Represents the ratio between the total number of pools and the wetted area extent within a section. Indicates the fragmentation of surface water (i.e. pools) for a given water extent.	• Indicates how fragmented a given water extent is and provides insights into the loss of pool connectivity.
Pool Longitudinal Fragmentation	$PLF = \frac{N}{\sum_{i=1}^{n} l_i}$	Pool/ km	Represents the ratio of the total number of pools and the section wetted length. Values increase as the pool's length gets smaller and the number of pools increase, indicating a higher likelihood of loss of longitudinal connectivity.	• Provides an insight into longitudinal connectivity/ fragmentation, which has implications for movement pathways for foraging, spawning, recolonization, or mass migration of aquatic fauna (e.g., diadromous fish and crustaceans).

Notation – $i = 1,\ldots,n$ *pool*/a_i = area of pool *i*/l_i = length of pool *i*/*N* = total number of pools in a section/*WP* = Sum of water observations through time for pixel/*T* = Total number of observations for pixel/*sa* = section total area/*sl* = river section length
Adapted from [1]McGarigal and Marks (1995).

Resilience describes the capacity of a system to recover after disturbance (i.e., drying) and was represented by six metrics: Pixel Persistence, Refuge Area, Wetted Area Percentage of Section, Wetted Length Percentage of Section, Pool Fragmentation and Pool Longitudinal Fragmentation. Pixel Persistence, Refuge Area, and Wetted Area Percentage of Section describe the amount of water within a section; hence are relevant to water persistence and hydrologic refugia. The Wetted Length Percentage of Section is the ratio between the sum of pool length within a section and section wetted length. While theoretically, values of this metric should not exceed 100 %, in reality, they can because while the section line length is fixed, the cumulative length of pools within the channel and in the floodplain within the buffer polygon can exceed this number. For instance, during the wet season, river pools may extend into adjacent floodplain creeks; alternatively, early in the dry season, multiple pools may exist side by side inside the main channel, i.e., the river channel is braided or contains anabranches. Pool Fragmentation and Pool Longitudinal Fragmentation are indicators of river fragmentation and are relevant to hydrological connectivity.

2.3.5. *Describing and evaluating hydrological attributes and derived metrics*

To visualize and understand patterns in attributes and metrics as the river system transitions from wet to dry, we fitted polynomial lines to our data. For any given attribute or metric (y), we created a regression model that predicted y given the day of the year (*day*). The global equation of the model is shown in Eq. (1), where day refers to the two composite samples per month ($n = 24$ per year). Polynomial terms were included for day, i.e., day^x, in recognition that metrics may display complex non-linear behavior through time.

$$Metric(y) = intercept + day + day^2 + day^3 + day^4 + \ldots day^6 \tag{1}$$

We fit linear models containing polynomial terms up to the 6th order using the Ordinary Least Squares (OLS) function in the package statsmodels (Seabold and Perktold, 2010) using a total of 478 observations for each model. This resulted in six models of increasing complexity with increasing polynomial terms. We used model selection to identify the model with best predictive capacity as we recognized that high-level polynomial terms may lead to overfitting (i.e., describing residual noise as opposed to true variation). Support for polynomial terms included in the global model were assessed by comparing model-subsets using the Akaike Information Criteria (AIC). AIC scores provide a measure of relative model support by trading off model fit (model likelihood) with model complexity, i.e., number of parameters (Burnham and Anderson, 2004). We model averaged parameters across all competing models with $\Delta AIC < 4.0$ as per Burnham and Anderson (2004) to produce the final model used for prediction (see supplement for AIC scores and ΔAIC values). Note that ΔAIC is the difference of the AIC score of each model from the best model (e.g., ΔAIC of the best model is 0). The same approach was used to describe seasonal changes among river sections. To explore the benefits of using metrics generated from imagery as opposed to a conventional gauged approach, we visually compared attribute and metric seasonal curves with rainfall and discharge graphs generated from two gauging stations (Noonkanbah and Looma).

It is important to highlight that Pixel Persistence and Refuge Area could not be analyzed using the approaches mentioned for the other metrics because these two metrics cannot be divided into time steps, i.e., their value is created from a temporal reduction. Still, we analyzed the differences in these metrics between sections. Note that the Pixel Persistence value used to describe any given river section was determined using the average value for the section, and the value for Refuge Area was based on the total area within a section. Furthermore, Pixel Persistence data were filtered, and all values <25 % discarded so that very low water observations and soils did not bias the metric mean.

3. Results

3.1. Hydrological attributes

The developed algorithm readily identified surface water in the main channel and the adjacent floodplain as well as the centerline of pools and their upstream and downstream ends (Fig. 4). Importantly, the algorithm generated values for pool area and perimeter that were the same as those calculated in ArcGIS 3.0. The algorithm's ability to identify pool length and endpoints also showed promising results upon visual inspection.

3.2. Attributes and metrics during drying and wetting phases

When combined across the five river sections, both attributes and metrics displayed considerable variation within a year, suggesting they were able to depict seasonal hydrologic patterns in the study area. During the wet season, there was a strong increase in pool total wetted area, perimeter and length (Fig. 5A–C). Changes in these attributes translated into a strong increase for metrics related to pool size (Fig. 5G–I), pool shape complexity (Fig. 5E), as well as metrics that described the percent coverage of water across a river section (Fig. 5K and L). The wet season created a strong decrease in metrics that described surface water fragmentation (Fig. 5L and M) and pool elongation (Fig. 5F); Note, smaller values represent more elongated pools for the Area-weighted Elongation Ratio metric. During the dry season, the opposite patterns were observed with pools becoming smaller, less complex and covering a smaller percent of the river section (Fig. 5E, G–J). Metrics describing pool length (Fig. 5H and K) declined more gently than those related to area or width (Fig. 5G–I), indicating that as the Fitzroy River dried, pools became narrower before they became shorter. As drying progressed pools became increasingly circular (Fig. 5F), as well as more fragmented (Fig. 5L and M).

Seasonal trends in attributes/metrics also identified the timing of peak changes in hydrology occurred. In the Fitzroy River, peak changes occurred during the middle/end of the wet season and the end of the dry/beginning of the wet season, as indicated by attributes and metrics displaying local maxima or minima at these times (Fig. 5). The rapid change during the middle to the end of the wet season reflected the transition of a river in flood with high connectivity to a non-flood state. The other period of rapid change during the end of the dry/beginning of the wet season presented the transition of the river from a series of shrinking pools in a fragmented channel back to a flooded connected state and translated into the opposite pattern for the attributes and metrics.

One attribute, the number of pools, displayed a complex seasonal pattern and is worthy of additional attention. This attribute showed three local maxima between mid to late wet and the mid-dry/early wet season and three local minima in the mid wet, early dry, and late dry season (Fig. 5D and Fig. 6B). The pattern arose because as the wet season progressed, river discharge (Fig. 5N) increased longitudinal connectivity, which caused the number of pools to decrease, i.e., see the first local minima in February (Fig. 6B – January Window – Note that 2018 had an early wet). As the wet season reached its peak and water extent was at its maximum, pools scattered across the floodplain were identified in the main channel buffer area (Fig. 6 – March Window) and the sum of these pools created the first local maxima in April (Fig. 6A and B). As flooding ended and the river started to fragment in the early dry season, the loss of ephemeral pools caused pool numbers to decrease rapidly (Fig. 6 – July Window), and the number of pools reached a second local minimum in July. As the dry season continued and the river fragmented further, larger pools split into several small pools, creating another set of local maxima in September. These small, fragmented pools continued to shrink as the dry season progressed until they ceased to exist, creating the last local minima in November. The number of pools continued to rise as the river fragmented further before the wet season commenced and improved hydrological connectivity in the early wet season (December) caused pools to join and their number to decrease again. A similar pattern was observed, albeit more muted, for the attribute Total Wetted Perimeter (Fig. 5B).

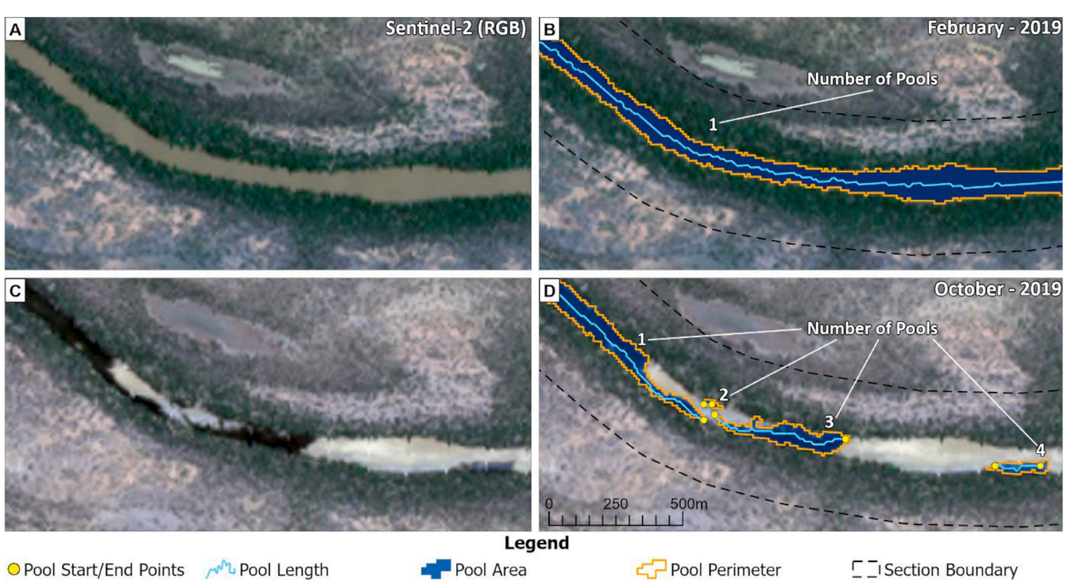

Fig. 4. An example of extracted attributes during the wet (A, B) and dry season (C, D). Left side images (A, C) represent the original RGB Sentinel-2 images, while the right side (B, D) also shows the extracted attributes. The dashed black lines represent the 250 m buffer. Note that the attribute pool length is shown with a light blue line, pool area is shown in dark blue, and pool perimeter is shown in orange. Attributes are determined for each continuous wetted area (i.e., pool). (For interpretation of the references to colour in this figure legend, the reader is referred to the web version of this article.)

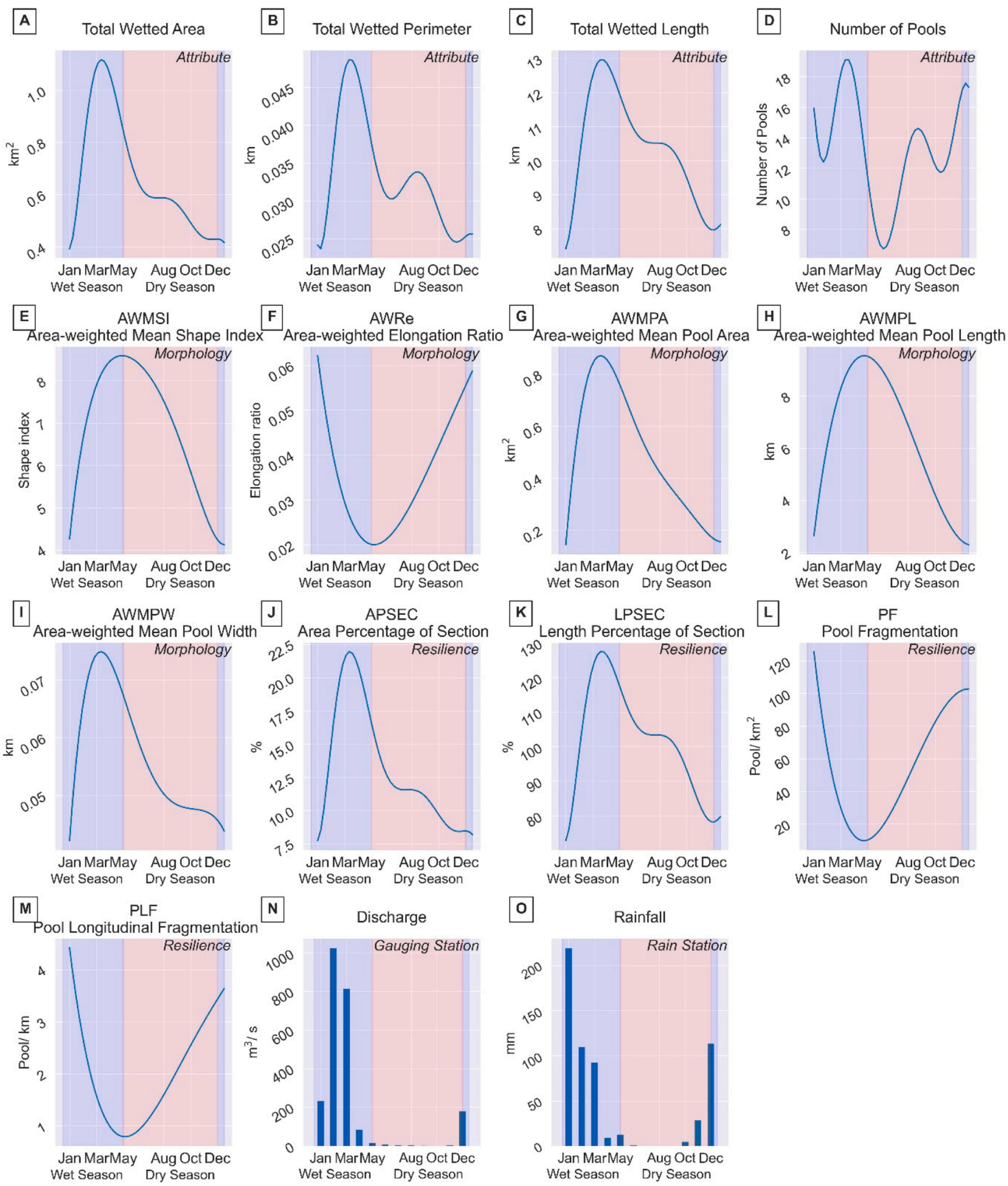

Fig. 5. Seasonal changes for each attribute and metric for all river sections combined. Each panel shows a different metric or attribute and whether the metric is relevant to morphology or resilience. The last two panels of the graph show monthly averaged gauged river discharge and rainfall. For each panel a light blue background indicates the wet season, and a pale red background indicates the dry season. (For interpretation of the references to colour in this figure legend, the reader is referred to the web version of this article.)

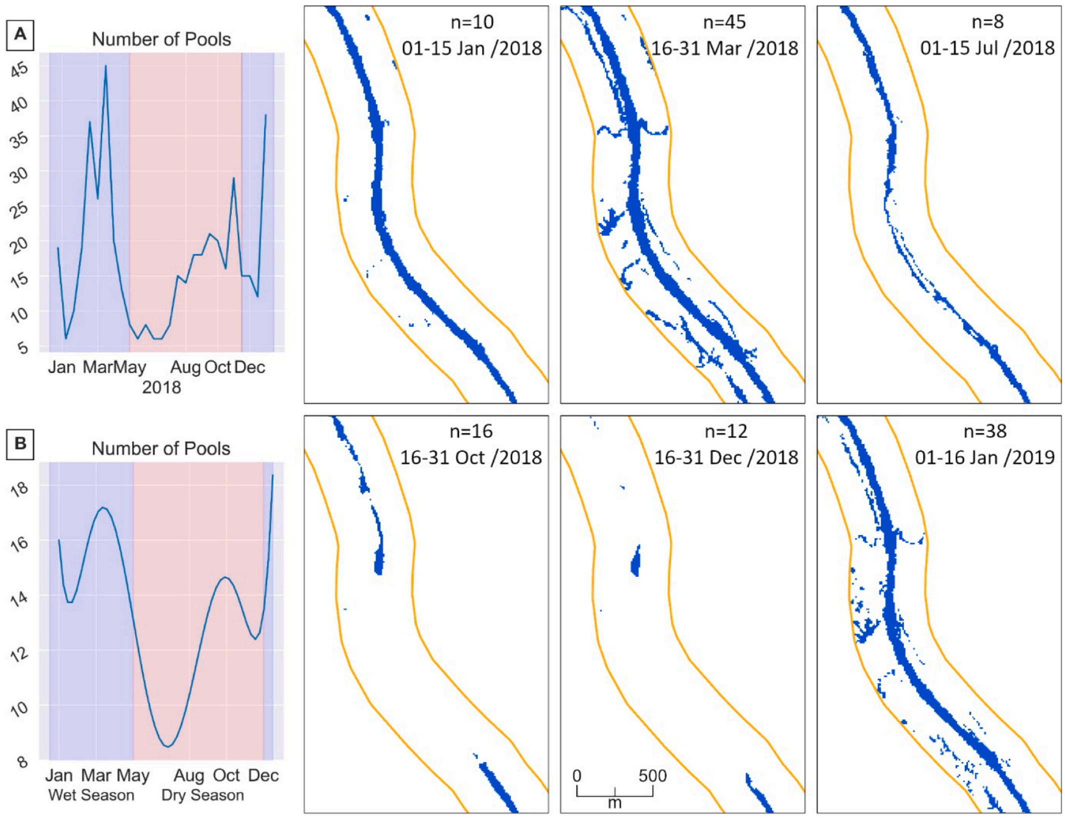

Fig. 6. An illustration of the temporal complexity of the attribute 'Number of Pools'. Panel A shows the attribute for Section 2 during a year with average rainfall (2018), Panel B shows the Number of Pools for all river sections for all study years. Windows to the right (top and bottom row) show the associated surface water mask for Section 2 during 2018 as the river transitions from wet season to dry and then back to wet. The total Number of Pools for Section 2 for each time period and the date range of the water masks are shown in the upper right corner of each window.

An examination of Fig. 5 also revealed that when the river stopped flowing in the dry season, and little or no information could be extracted from gauged data (Fig. 5N), our spatial metrics kept tracking hydrological characteristics of the river sections analyzed. Mean monthly total rainfall data (Fig. 5O) also assists our interpretation of the general behavior of the metrics by providing information on the intensity and temporal distribution of rainfall events.

3.3. *Attributes and metrics within river sections of varying persistence and fragmentation*

The seasonal patterns identified above were also observed independently in each river section, but their magnitude was highly variable between the five sections in line with their hydrological persistence. For instance, typically the more hydrological persistent the section the smoother and less steep the attribute or metric curve over time; conversely, the less persistent the section the more abrupt the curve decay with a steeper slope (Fig. 7). More subdued seasonal changes were particularly evident for pool number and length (Fig. 7D and C) and for metrics linked to fragmentation (Fig. 7L and M), pool elongation (Fig. 7F) or length as a percentage of river section (Fig. 7K). These pattern emerged because river sections with relatively persistent surface water, potentially due to high groundwater inputs, demonstrated less variation in surface water extent, hence attribute and metric values over time, than river sections with little to no groundwater inputs. Exceptions in the general pattern did emerge, especially for metrics linked to pool area or width (Fig. 7G and I).

Attribute and metric values also differed considerably for river sections with different hydrological persistence, indicating that metrics were adept at representing spatial differences in hydrology. For instance, river sections with low hydrological persistence (sections 1 and 2) had pools which were smaller in size (i.e. area, length, width, percentage of landscape) during both the wet and dry season compared to those in sections with potential stronger links to groundwater (sections 3–5) (Fig. 7G–J). Further, river sections with low persistence contained more pools (Fig. 7D) that were cut off from one another (Fig. 7L and M) and covered a smaller portion of the channel (Fig. 7J) compared to river sections with high persistence.

Metrics that directly described hydrological persistence also depicted differences among river sections indicating that they were also adept at identifying hydrological differences. For instance, values for Pixel Persistence and Refuge Area were considerably higher in river sections with a high likelihood of groundwater inputs (sections 4 and 5) and were lower in sections of the river with minimal likelihood of groundwater inputs (sections 1 and 2) (Fig. 8A and B; Fig. 9). Refuge Area, which only includes values of Pixel Persistence above 90 %, was the more sensitive of the two metrics and differed by two orders of magnitude between sections 1 and 2 and sections 3 to 5, with values of 0.0019 and 0.0207 for the former and >0.25 for the latter (Fig. 8B). Pixel Persistence was less sensitive, with a maximum difference of only 17 % between the most different river sections, i.e., 1 and 5 (Fig. 8A).

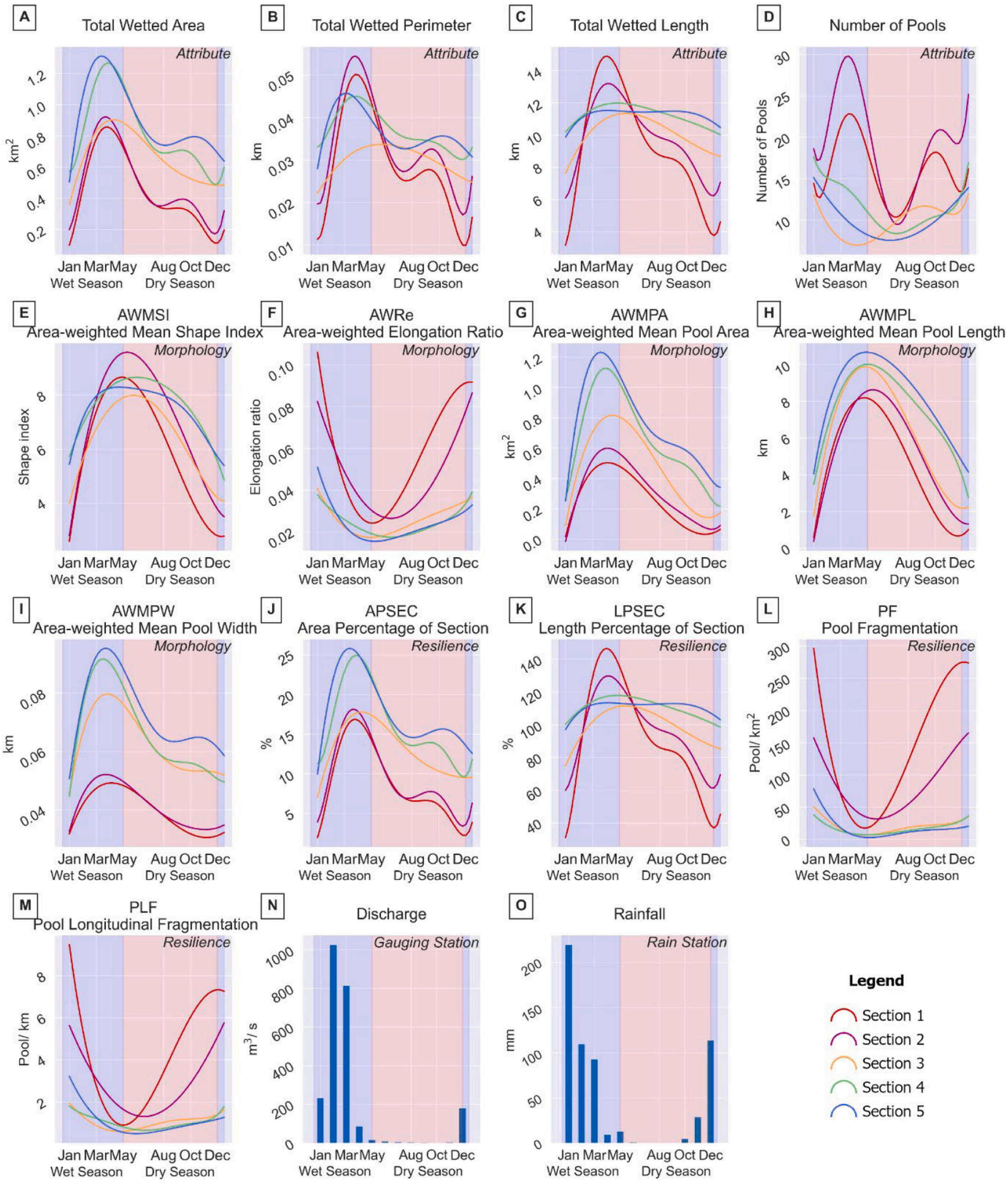

Fig. 7. Seasonal changes among river sections for each attribute and metric. Each panel shows a different metric or attribute and whether the metric contributes to understanding morphology or resilience. The last two panels of the graph show monthly averaged gauged river discharge and rainfall. For each panel, a light blue background indicates the wet season and a pale red background indicates the dry season. (For interpretation of the references to colour in this figure legend, the reader is referred to the web version of this article.)

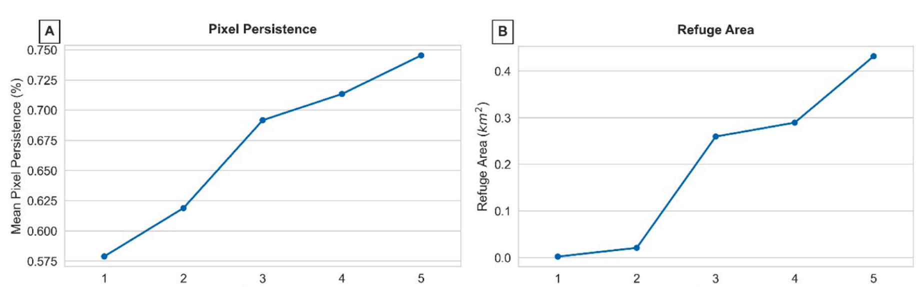

Fig. 8. Line graphs showing A: Mean Pixel Persistence and B: Total Refuge Area for each section.

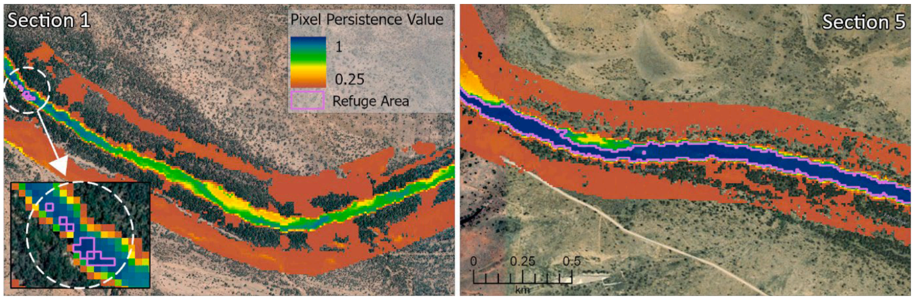

Fig. 9. Example of the difference between Pixel Persistence and Refuge Area between sections one and five. Note, the white dashed circle on left side of Section 1 zooms in on the Refuge Area in this section.

4. Discussion

This study demonstrated that hydrological attributes and metrics automatically derived from multispectral imagery can accurately describe aspects of an intermittent river's hydrology and have the potential to provide meaningful insights into river morphology, resilience, and ecological functioning. Metrics proved effective at describing seasonal patterns, revealing how the size, complexity and elongation of surface water features (e.g., pools) decreased as the study river transitioned from wet to dry and how fragmentation increased. Metrics also enabled the differentiation of river sections with varied hydrological persistence. Using remotely sensed technology with automated algorithms to characterize the hydrology of intermittent rivers is a significant advance and has the potential to increase our understanding of remote and understudied rivers and improve their management.

Characterizing surface water hydrology in intermittent rivers can help us generate and transfer knowledge, assess impacts and monitor recovery (Kennard et al., 2010; Olden et al., 2012). For instance, knowledge will be generated when metrics are used to identify refuge locations in a river system or map the extent of aquatic habitats, i.e., floodplain, main channel, tributary, and estuarine. Knowledge generation can also be facilitated by using metrics as covariates in predictive models, improving our ability to investigate hydrological and ecological relationships (Beesley et al., 2014; Canham et al., 2021; King et al., 2016). Characterizing a river using remotely sensed metrics rather than gauged discharge data or hydrodynamic models provides another lens to evaluate hydrology (as per Olden et al., 2012) and may improve our ability to transfer knowledge among river systems within a region, among regions and potentially among continents. It could also be incorporated into approaches that seek to protect the natural flow regime in the face of development, such as the ecological limits of hydrologic alteration (ELOHA) framework (Poff et al., 2010). The remotely sensed attributes and metrics presented in this study can also help quantify the impacts of threats, such as water resource development (i.e., the construction of impoundments, surface or subsurface water extraction), land use change and climate change. Lastly, attributes and metrics can play an important role in quantifying the effect of restorative actions. For instance, metrics can be used to assess environmental water delivery (also known as experimental floods) by mapping changes in the size of aquatic habitats or could be used to quantify hydrologic changes that result from altered dam operation rules or the removal of infrastructure.

Although our attributes and ecohydrological metrics show much promise, a multispectral approach is not without challenges. Firstly, the quality of the metrics depend directly on the quality of the water identification process, which is limited by the configuration of the Water Detect algorithm (Cordeiro et al., 2021; Tayer et al., 2023) and a range of other factors associated with the spatial resolution of the image data, satellite return time and land cover variability. In this study, the accuracy of the water identification process is expected to have achieved similarly good results as reported by Tayer et al. (2023) since we used the recommended optimum time-averaged input parameters (i.e., water indices combination, maximum clustering, and regularization) for the Water Detect algorithm (Cordeiro et al., 2021) and applied them in the same catchment. While this is encouraging, it is important to note that the spatial resolution of the image data influences the level of detail of the water mask, thus Sentinel-2 data (10 m pixels) may be too coarse to provide meaningful imagery for narrow intermittent waterways, such as tributary streams. It may also preclude mapping of small aquatic features, such as riffles, which are common in intermittent rivers. The 5-day return cycle of Sentinel-2 may also limit its ability to characterize brief hydrological events, making it difficult to describe flashy rainfall-runoff responses which are likely to occur in headwater streams or in systems with relatively impermeable substrates. In addition, this technique may not be applicable in regions with frequent cloud cover if using Sentinel-2. However, one of the benefits of using our approach is that it can be applied to any multispectral image with at least Visible + Near-infrared bands. Choosing satellites with quick return, such as Planetscope and Worldview, can help avoid cloud cover issues. Land cover can also affect the process of water identification since heavily shadowed, burnt, and urban areas can influence the accuracy of common water indices such as the Normalized Difference Water Index (NDWI) and Modified Normalized Difference Water Index (MNDWI) (Guo et al., 2017; Xu, 2006; Zhai et al., 2015; Zhang et al., 2011), used in the Water Detect algorithm. For this reason, a preliminary visual exploratory analysis of the study area is strongly recommended to evaluate the best combination of spectral bands for any use case. Importantly, if the water mask is accurate, the process of extracting attributes should be straightforward and produce reliable results. Another challenge, although not observed in this study, is the possibility that pool length can be underestimated if the river channel bends strongly and pool endpoints lie close together (in Euclidean distance). Differences in topography among river sections may also influence a multispectral characterization of hydrology. For instance, some sections may have fewer topographic depressions than others and therefore form fewer ephemeral pools. Lastly, the use of a buffer zone around a river centerline to characterize a river channel, while pragmatic and timesaving, has the potential to introduce error into metrics if the aim is the evaluate the main channel only, as surface water on the adjacent floodplain may also be included. This type of error can be countered by changing the buffer distance when configuring the algorithm or by providing the exact main channel boundary.

For those seeking to use our multispectral approach, careful consideration must be given to the choice of parameters used as input for the water identification process. We recommend using the sensitivity test developed by Tayer et al.'s (2023), as it was specifically designed to identify the best parameters for the Water Detect algorithm. The test compares the results of a combination of input parameters to determine values that reflect the most accurate water mask for each use case. Although this technique requires ground-truthed or remotely interpreted data for its accuracy assessment, we recommend its use because results can improve dramatically if adopted. However, for those unable to obtain ground-truthed data, we note that, in some cases, good results can still be achieved using the Water Detect default parameters (Cordeiro et al., 2021; Tayer et al., 2023; Tottrup et al., 2022). Importantly, our algorithm to generate attributes and metrics has been developed in modules, thus can be easily updated if more accurate methods to detect water arise.

A multispectral approach to characterizing the hydrology of intermittent rivers offers much promise, but its advantages and usefulness will only be revealed by trialing its use. We encourage others to use this method for the range of potential applications mentioned earlier. We are especially keen to see its ability to characterize the similarity of riverine sections within a catchment as well as its ability to characterize hydrology among river systems. Studies that are able to acquire long time series imagery (i.e., decadal) will be able to investigate links between climate and hydrology and may shed new light on our understanding of the impacts of climate change on intermittent river systems. Such an approach may be achieved using the Landsat satellite series which has been around since the 1970′s; however, the reduced spatial resolution of Landsat imagery means that we recommend this approach only for river sections with wide channels. We also welcome studies comparing and contrasting hydrological characterizations based on this spatial method with those using gauged discharge data, as per Olden et al. (2012) and Kennard et al. (2010), as revealing differences may showcase the strength of a spatial approach and potentially reveal its limitations. Studies that link metrics to ecological patterns or processes will reveal their ecological relevance and limitations and are fundamentally important. Lastly, we encourage others to test the developed algorithm and the resulting attributes and metrics in their intermittent rivers and report back. Only through trialing the method across a range of river systems will its advantages and limitations become clear. This process will inevitably lead to metric refinement, the addition of other metrics, and recommendations about where metrics are most useful.

5. Conclusion

In this study, we developed a suite of ecohydrological attributes and metrics to characterize intermittent rivers over time that uses multiple multispectral images as input. The process of calculating attributes and metrics has been automated in an open-source algorithm built in a Python 3.7 environment. The source line of code is available on GitHub for community editing and improvement via collaboration (see Data Availability Statement), making the algorithm conveniently accessible for future users. Our case study indicated that the attributes and metrics were highly effective in characterizing the morphology and resilience of river sections and highlighting their relative hydrological differences. Our approach has great potential to be implemented because the developed algorithm has been designed to be easily used by professionals from different areas, such as hydrology, hydrogeology, ecology, climatology, and management, so long as the user has programming skills. A better understanding of intermittent rivers' hydrological characteristics and how they change through space and time is useful for resource assessments, water allocation planning, management prioritization (e.g., identification of refuge locations) and climate change studies. By improving knowledge generation and decision-making, this hydrologic tool will contribute to the management and protection of intermittent rivers.

CRediT authorship contribution statement

Thiaggo C. Tayer: Conceptualization, Methodology, Software, Writing – original draft, Writing – review & editing, Visualization. **Leah S. Beesley:** Conceptualization, Writing – original draft, Writing – review & editing. **Michael M. Douglas:** Conceptualization, Writing – review & editing. **Sarah A. Bourke:** Writing – review & editing. **J. Nik Callow:** Writing – review & editing. **Karina Meredith:** Writing – review & editing. **Don McFarlane:** Writing – review & editing.

Declaration of Competing Interest

The authors declare that they have no known competing financial interests or personal relationships that could have appeared to influence the work reported in this paper.

Data availability

Data will be made available on request.

Acknowledgments

This project was carried out as part of the lead author's PhD research, with financial support from the Australian Government's Research Training Program (RTP), the National Environmental Science Program (NESP) through its Northern Australia Environmental Resources Hub (Project 1.3.3), and the Australian Institute of Nuclear Science and Engineering through the Postgraduate Research Awards (PGRA - ALNSTU12627).

Appendix A. Supplementary data

Supplementary data to this article can be found online at https://doi.org/10.1016/j.jhydrol.2023.129087.

References

Acuña, V., Datry, T., Marshall, J., Barceló, D., Dahm, C.N., Ginebreda, A., McGregor, G., Sabater, S., Tockner, K., Palmer, M.A., 2014. Why should we care about temporary waterways? Science 1979 (343), 1080–1081. https://doi.org/10.1126/science.1246666.

Beesley, L.S., Gwinn, D.C., Price, A., King, A.J., Gawne, B., Koehn, J.D., Nielsen, D.L., Crispo, E., 2014. Juvenile fish response to wetland inundation: how antecedent conditions can inform environmental flow policies for native fish. Journal of Applied Ecology 51 (6), 1613–1621.

Beesley, L.S., Pusey, B.J., Douglas, M.M., Keogh, C.S., Kennard, M.J., Canham, C.A., Close, P.G., Dobbs, R.J., Setterfield, S.A., 2021. When and where are catfish fat fish? Hydro-ecological determinants of energy reserves in the fork-tailed catfish, Neoarius graeffei, in an intermittent tropical river. Freshw Biol 66, 1211–1224. https://doi.org/10.1111/FWB.13711.

Beven, K.J., Wood, E.F., Sivapalan, M., 1988. On hydrological heterogeneity — Catchment morphology and catchment response. J Hydrol (Amst) 100, 353–375. https://doi.org/10.1016/0022-1694(88)90192-8.

Blackman, R.C., Altermatt, F., Foulquier, A., Lefébure, T., Gauthier, M., Bouchez, A., Stubbington, R., Weigand, A.M., Leese, F., Datry, T., 2021. Unlocking our understanding of intermittent rivers and ephemeral streams with genomic tools. Front Ecol Environ 19, 574–583. https://doi.org/10.1002/FEE.2404.

Bond, N.R., Kennard, M.J., 2017. Prediction of Hydrologic Characteristics for Ungauged Catchments to Support Hydroecological Modeling. Water Resour Res 53, 8781–8794. https://doi.org/10.1002/2017WR021119.

Boulton, A.J., 2014. Conservation of ephemeral streams and their ecosystem services: what are we missing? Aquat Conserv 24, 733–738. https://doi.org/10.1002/aqc.2537.

Bradski, G., 2000. The OpenCV Library.

Bunn, S.E., Thoms, M.C., Hamilton, S.K., Capon, S.J., 2006. Flow variability in dryland rivers: boom, bust and the bits in between. River Res Appl 22, 179–186. https://doi.org/10.1002/rra.904.

Burnham, K.P., Anderson, D.R., 2004. Multimodel Inference: Understanding AIC and BIC in Model Selection. Sociol Methods Res 33, 261–304. https://doi.org/10.1177/0049124104268644.

Callow, J.N., Boggs, G.S., 2013. Studying reach-scale spatial hydrology in ungauged catchments. J Hydrol (Amst) 496, 31–46. https://doi.org/10.1016/J.JHYDROL.2013.05.030.

Callow, J.N., Smettem, K.R.J., 2009. The effect of farm dams and constructed banks on hydrologic connectivity and runoff estimation in agricultural landscapes. Environmental Modelling & Software 24, 959–968. https://doi.org/10.1016/J.ENVSOFT.2009.02.003.

Callow, J.N., van Niel, K.P., Boggs, G.S., 2007. How does modifying a DEM to reflect known hydrology affect subsequent terrain analysis? J Hydrol (Amst) 332, 30–39. https://doi.org/10.1016/J.JHYDROL.2006.06.020.

Canham, C.A., Beesley, L.S., Gwinn, D.C., Douglas, M.M., Setterfield, S.A., Freestone, F. L., Pusey, B.J., Loomes, R.C., 2021. Predicting the occurrence of riparian woody species to inform environmental water policies in an Australian tropical river. Freshw Biol 66, 2251–2263. https://doi.org/10.1111/FWB.13829.

Charles, S., Petheram, C., Berthet, A., Browning, G., Hodgson, G., Wheeler, M., Yang, A., Gallant, S., Vaze, J., Wang, B., Marshall, A., Hendon, H., Kuleshov, Y., Dowdy, A., Reid, P., Read, A., Feikema, P., Hapuarachchi, P., Smith, T., Gregory, P., Shi, L., 2016. Climate data and their characterisation for hydrological and agricultural scenario modelling across the Fitzroy. Darwin and Mitchell catchments. https://doi.org/10.25919/5B86ED38D15A6.

Chiu, M.C., Leigh, C., Mazor, R., Cid, N., Resh, V., 2017. Anthropogenic Threats to Intermittent Rivers and Ephemeral Streams. Intermittent Rivers and Ephemeral Streams: Ecology and Management 433–454. https://doi.org/10.1016/B978-0-12-803835-2.00017-6.

Cordeiro, M.C.R., Martinez, J.M., Peña-Luque, S., 2021. Automatic water detection from multidimensional hierarchical clustering for Sentinel-2 images and a comparison with Level 2A processors. Remote Sens Environ 253, 112209. https://doi.org/10.1016/J.RSE.2020.112209.

Crowley, M.A., Cardille, J.A., 2020. Remote Sensing's Recent and Future Contributions to Landscape Ecology. Current Landscape Ecology Reports. Curr Landscape Ecol Rep 5 (3), 45–57.

D'Ambrosio, E., de Girolamo, A.M., Barca, E., Ielpo, P., Rulli, M.C., 2017. Characterising the hydrological regime of an ungauged temporary river system: a case study. Environmental Science and Pollution Research 24, 13950–13966. https://doi.org/10.1007/S11356-016-7169-0/FIGURES/4.

Dask Development Team, 2016. Dask: Library for dynamic task scheduling.

Datry, T., Larned, S.T., Tockner, K., 2014. Intermittent Rivers: A Challenge for Freshwater Ecology. Bioscience 64, 229–235. https://doi.org/10.1093/BIOSCI/BIT027.

Datry, T., Bonada, N., Boulton, A., 2017. Intermittent Rivers and Ephemeral Streams, 1st Edition. ed. Academic Press.

Frasson, R.P.d.M., Pavelsky, T.M., Fonstad, M.A., Durand, M.T., Allen, G.H., Schumann, G., Lion, C., Beighley, R.E., Yang, X., 2019. Global Relationships Between River Width, Slope, Catchment Area, Meander Wavelength, Sinuosity, and Discharge. Geophys Res Lett 46 (6), 3252–3262.

Gitz, D., Zartman, R., Villarreal, C., Rainwater, K., Smith, L., Ritchie, G., 2015. Sediment Accumulation in Semi-arid Wetlands of the Texas Southern High Plains. Texas Jornal of Agriculture and Natural Resources 28, 70–81.

Guo, Q., Pu, R., Li, J., Cheng, J., 2017. A weighted normalized difference water index for water extraction using Landsat imagery. Int J Remote Sens 38, 5430–5445. https://doi.org/10.1080/01431161.2017.1341667.

Harrington, G.A., Harrington, N.M., 2015. Lower Fitzroy River Groundwater Review. A report prepared by Innovative Groundwater Solutions for Department of Water, 15 May 2015.

Harrington, G.A., Harrington, N.M., 2016. A preliminary assessment of groundwater contribution to wetlands in the lower reaches of Fitzroy River catchment. A report prepared for Department of Water, Western Australia by Innovative Groundwater Solutions.

Harrington, G.A., Stelfox, L., Gardner, P., Davies, P., Doble, R., Cook, P., 2011. Surface Water – Groundwater Interactions in the Lower Fitzroy River, Western Australia. CSIRO: Water for a Healthy Country. National Research Flagship 54.

Hermosilla, T., Wulder, M.A., White, J.C., Coops, N.C., Pickell, P.D., Bolton, D.K., 2019. Impact of time on interpretations of forest fragmentation: Three-decades of fragmentation dynamics over Canada. Remote Sens Environ 222, 65–77. https://doi.org/10.1016/J.RSE.2018.12.027.

Hoyer, S., Hamman, J., 2017. xarray: N-D labeled Arrays and Datasets in Python. J Open Res Softw 5 (1), 10.

Jarihani, A.A., Callow, J.N., McVicar, T.R., Van Niel, T.G., Larsen, J.R., 2015. Satellite-derived Digital Elevation Model (DEM) selection, preparation and correction for hydrodynamic modelling in large, low-gradient and data-sparse catchments. Journal of Hydrology 524, 489–506. https://doi.org/10.1016/j.jhydrol.2015.02.049.

Kennard, M.J., Pusey, B.J., Olden, J.D., MacKay, S.J., Stein, J.L., Marsh, N., 2010. Classification of natural flow regimes in Australia to support environmental flow management. Freshw Biol 55, 171–193. https://doi.org/10.1111/J.1365-2427.2009.02307.X.

King, A.J., Gwinn, D.C., Tonkin, Z., Mahoney, J., Raymond, S., Beesley, L., Heino, J., 2016. Using abiotic drivers of fish spawning to inform environmental flow management. Journal of Applied Ecology 53 (1), 34–43. https://doi.org/10.1111/1365-2664.12542.

Koundouri, P., Boulton, A.J., Datry, T., Souliotis, I., 2017. Ecosystem Services, Values, and Societal Perceptions of Intermittent Rivers and Ephemeral Streams. Intermittent Rivers and Ephemeral Streams: Ecology and Management 455–476. https://doi.org/10.1016/B978-0-12-803835-2.00018-8.

Larkin, Z.T., Ralph, T.J., Tooth, S., Fryirs, K.A., Carthey, A.J.R., 2020. Identifying threshold responses of Australian dryland rivers to future hydroclimatic change. Sci Rep 10 (1). https://doi.org/10.1038/s41598-020-63622-3.

Lee, T.C., Kashyap, R.L., Chu, C.N., 1994. Building Skeleton Models via 3-D Medial Surface Axis Thinning Algorithms. CVGIP: Graphical Models and Image. Processing 56 (6), 462–478. https://doi.org/10.1006/cgip.1994.1042.

Li, F., Lymburner, L., Mueller, N., Tan, P., Islam, A., Jupp, D.L.B., Reddy, S., 2010. An Evaluation of the Use of Atmospheric and BRDF Correction to Standardize Landsat Data. IEEE J Sel Top Appl Earth Obs Remote Sens 3, 257–270. https://doi.org/10.1109/JSTARS.2010.2042281.

Li, F., Jupp, D.L.B., Thankappan, M., Lymburner, L., Mueller, N., Lewis, A., Held, A., 2012. A physics-based atmospheric and BRDF correction for Landsat data over mountainous terrain. Remote Sens Environ 124, 756–770. https://doi.org/10.1016/J.RSE.2012.06.018.

McGarigal, K., Marks, B.J., 1995. FRAGSTATS: spatial pattern analysis program for quantifying landscape structure. Gen. Tech. Rep. PNW-GTR-351. Portland, OR: U.S. Department of Agriculture, Forest Service, Pacific Northwest Research Station. 122 p 351. https://doi.org/10.2737/PNW-GTR-351.

Messager, M.L., Lehner, B., Cockburn, C., Lamouroux, N., Pella, H., Snelder, T., Tockner, K., Trautmann, T., Watt, C., Datry, T., 2021. Global prevalence of non-perennial rivers and streams. Nature 594 (7863), 391–397. https://doi.org/10.1038/s41586-021-03565-5.

Olariu, B., Vîrghileanu, M., Mihai, B.-A., Săvulescu, I., Toma, L., Săvulescu, M.-G., 2022. Forest Habitat Fragmentation in Mountain Protected Areas Using Historical Corona KH-9 and Sentinel-2 Satellite Imagery. Remote Sensing 14 (11), 2593. https://doi.org/10.3390/rs14112593.

Olden, J.D., Kennard, M.J., Pusey, B.J., 2012. A framework for hydrologic classification with a review of methodologies and applications in ecohydrology. Ecohydrology 5, 503–518. https://doi.org/10.1002/ECO.251.

Petheram, C., Bruce, C., Chilcott, C., Campbell, S.T., Watson, I., 2018. Water resource assessment for the Fitzroy catchment. A report to the Australian Government from the CSIRO Northern Australia Water Resource Assessment, part of the National Water Infrastructure Development Fund: Water Resource Assessments. CSIRO, Australia.

Poff, N.L., Richter, B.D., Arthington, A.H., Bunn, S.E., Naiman, R.J., Kendy, E., Acreman, M., Apse, C., Bledsoe, B.P., Freeman, M.C., Henriksen, J., Jacobson, R.B., Kennen, J.G., Merritt, D.M., O'Keefee, J.H., Olden, J.D., Rogers, K., Tharme, R.E., Warner, A., 2010. The ecological limits of hydrologic alteration (ELOHA): a new framework for developing regional environmental flow standards. Freshw Biol 55, 147–170. https://doi.org/10.1111/j.1365-2427.2009.02204.x.

Pollino, C., Buckworth, R., Barber, E., Cadiegues, M., Deng, R., Ebner, B., Kenyon, R., Liedloff, A., Merrin, L., Moeseneder, C., Morgan, D., Nielsen, D., O'Sullivan, J., Ponce Reyes, R., Robson, B., Stratford, D., Stewart-Koster, B., Turschwell, M., 2018. Synthesis of knowledge to support the assessment of impacts of water resource development to ecological assets in northern Australia: asset descriptions. CSIRO, Canberra. https://doi.org/10.25919/5B86ED9B99563.

Pringle, C.M., 2001. Hydrologic Connectivity and the Management of Biological Reserves: A Global Perspective. Ecology Applications 11 (4), 981–998. https://doi.org/10.2307/3061006.

Pringle, C., 2010. Hydrologic connectivity: a neglected dimension of conservation biology. In: Crooks, K.R., Sanjayan, M. (Eds.), Connectivity Conservation. Cambridge University Press, pp. 233–254.

Reddy, G.P., Maji, A.K., Gajbhiye, K.S., 2004. Drainage morphometry and its influence on landform characteristics in a basaltic terrain, Central India – a remote sensing and GIS approach. International Journal of Applied Earth Observation and Geoinformation 6, 1–16. https://doi.org/10.1016/J.JAG.2004.06.003.

Richter, B.D., Baumgartner, J.V., Powell, J., Braun, D.P., 1996. A Method for Assessing Hydrologic Alteration within Ecosystems. Conservation Biology 10 (4), 1163–1174.

Roach, K.A., Winemiller, K.O., Davis, S.E., 2014. Autochthonous production in shallow littoral zones of five floodplain rivers: effects of flow, turbidity and nutrients. Freshw Biol 59 (6), 1278–1293. https://doi.org/10.1111/fwb.12347.

Schumm, S.A., 1956. Evolution of drainage systems and slopes in badlands at Perth Amboy, New Jersey. Geological Society of American Bulletin 67, 597–646 https://doi.org/https://doi.org/10.1130/0016-7606(1956)67[597:EODSAS]2.0.CO;2.

Seabold, S., Perktold, J., 2010. Statsmodels: Econometric and Statistical Modeling with Python. Proceedings of the 9th Python in Science Conference.

Shanafield, M., Bourke, S.A., Zimmer, M.A., Costigan, K.H., 2021. An overview of the hydrology of non-perennial rivers and streams. Wiley Interdisciplinary Reviews: Water 8, e1504. https://doi.org/10.1002/wat2.1504.

Sims, N., Anstee, J., Barron, O., Botha, H., Lehmann, E., Li, L., McVicar, T., Paget, M., Ticehurst, C., van Niel, T., Warren, Garth., 2016. Earth observation remote sensing. A technical report to the Australian Government from the CSIRO Northern Australia Water Resource Assessment, part of the National Water Infrastructure Development Fund: Water Resource Assessments. CSIRO, Australia. doi:10.25919/5b86edb95a4de.

Smettem, K.R.J., Waring, R.H., Callow, J.N., Wilson, M., Mu, Q., 2013. Satellite-derived estimates of forest leaf area index in southwest Western Australia are not tightly coupled to interannual variations in rainfall: implications for groundwater decline in a drying climate. Glob Chang Biol 19, 2401–2412. https://doi.org/10.1111/GCB.12223.

Taylor, A.R., Harrington, G.A., Clohessy, S., Dawes, W.R., Crosbie, R.S., Doble, R.C., Wohling, D.L., Batlle-Aguilar, J., Davies, P.J., Thomas, M., Suckow, A., 2018. Hydrogeological assessment of the Grant Group and Poole Sandstone-Fitzroy catchment, Western Australia. A technical report to the Australian Government from the CSIRO Northern Australia Water Resource Assessment, part of the National Water Infrastructure Development Fund: Water Resource Assessments. CSIRO, Australia. doi:10.25919/5b86ed7e26b48.

Tayer, T.C., Douglas, M.M., Cordeiro, M.C.R., Tayer, A.D.N., Callow, J.N., Beesley, L.S., McFarlane, D., 2023. Improving the accuracy of the Water Detect algorithm using Sentinel-2, Planetscope and Sharpened imagery: a case study in an intermittent river. GIScience & Remote Sensing.

Tottrup, C., Druce, D., Meyer, R.P., Christensen, M., Riffler, M., Dulleck, B., Rastner, P., Jupova, K., Sokoup, T., Haag, A., Cordeiro, M.C.R., Martinez, J.-M., Franke, J., Schwarz, M., Vanthof, V., Liu, S., Zhou, H., Marzi, D., Rudiyanto, R., Thompson, M., Hiestermann, J., Alemohammad, H., Masse, A., Sannier, C., Wangchuk, S., Schumann, G., Giustarini, L., Hallowes, J., Markert, K., Paganini, M., 2022. Surface Water Dynamics from Space: A Round Robin Intercomparison of Using Optical and SAR High-Resolution Satellite Observations for Regional Surface Water Detection. Remote Sensing 14 (10), 2410. https://doi.org/10.3390/rs14102410.

van der Walt, S., Schönberger, J.L., Nunez-Iglesias, J., Boulogne, F., Warner, J.D., Yager, N., Gouillart, E., Yu, T., 2014. Scikit-image: Image processing in python. PeerJ 2014. https://doi.org/10.7717/PEERJ.453/FIG-1.

Vincenty, T., 1975. Direct and inverse solutions of geodesics on the ellipsoid with application of nested equations. Survey Review 23, 88–93. https://doi.org/10.1179/sre.1975.23.176.88.

Virtanen, P., Gommers, R., Oliphant, T.E., Haberland, M., Reddy, T., Cournapeau, D., Burovski, E., Peterson, P., Weckesser, W., Bright, J., van der Walt, S.J., Brett, M., Wilson, J., Millman, K.J., Mayorov, N., Nelson, A.R.J., Jones, E., Kern, R., Larson, E., Carey, C.J., Polat, İ., Feng, Y.u., Moore, E.W., VanderPlas, J., Laxalde, D., Perktold, J., Cimrman, R., Henriksen, I., Quintero, E.A., Harris, C.R., Archibald, A. M., Ribeiro, A.H., Pedregosa, F., van Mulbregt, P., Vijaykumar, A., Bardelli, A.P., Rothberg, A., Hilboll, A., Kloeckner, A., Scopatz, A., Lee, A., Rokem, A., Woods, C.N., Fulton, C., Masson, C., Häggström, C., Fitzgerald, C., Nicholson, D.A., Hagen, D.R., Pasechnik, D.V., Olivetti, E., Martin, E., Wieser, E., Silva, F., Lenders, F., Wilhelm, F., Young, G., Price, G.A., Ingold, G.-L., Allen, G.E., Lee, G.R., Audren, H., Probst, I., Dietrich, J.P., Silterra, J., Webber, J.T., Slavič, J., Nothman, J., Buchner, J., Kulick, J., Schönberger, J.L., de Miranda Cardoso, J.V., Reimer, J., Harrington, J., Rodríguez, J.L.C., Nunez-Iglesias, J., Kuczynski, J., Tritz, K., Thoma, M., Newville, M., Kümmerer, M., Bolingbroke, M., Tartre, M., Pak, M., Smith, N.J., Nowaczyk, N., Shebanov, N., Pavlyk, O., Brodtkorb, P.A., Lee, P., McGibbon, R.T., Feldbauer, R., Lewis, S., Tygier, S., Sievert, S., Vigna, S., Peterson, S., More, S., Pudlik, T., Oshima, T., Pingel, T.J., Robitaille, T.P., Spura, T., Jones, T.R., Cera, T., Leslie, T., Zito, T., Krauss, T., Upadhyay, U., Halchenko, Y.O., Vázquez-Baeza, Y., 2020. SciPy 1.0: fundamental algorithms for scientific computing in Python. Nat Methods 17 (3), 261–272.

Ward, J.V., Tockner, K., Arscott, D.B., Claret, C., 2002. Riverine landscape diversity. Freshw Biol 47 (4), 517–539.

Winfield, I.J., 2004. Fish in the littoral zone: ecology, threats and management. Limnologica 34, 124–131. https://doi.org/10.1016/S0075-9511(04)80031-8.

Xu, H., 2006. Modification of normalised difference water index (NDWI) to enhance open water features in remotely sensed imagery. Int J Remote Sens 27, 3025–3033. https://doi.org/10.1080/01431160600589179.

Yuan, X. zhong, Zhang, Y. wei, Liu, H., Xiong, S., Li, B., Deng, W., 2013. The littoral zone in the Three Gorges Reservoir, China: Challenges and opportunities. Environmental Science and Pollution Research 20, 7092–7102. https://doi.org/10.1007/S11356-012-1404-0/FIGURES/8.

Zhai, K., Wu, X., Qin, Y., Du, P., 2015. Comparison of surface water extraction performances of different classic water indices using OLI and TM imageries in different situations. Geo-spatial Information Science 18, 32–42. https://doi.org/10.1080/10095020.2015.1017911.

Zhang, F.F., Zhang, B., Li, J.S., Shen, Q., Wu, Y., Song, Y., 2011. Comparative Analysis of Automatic Water Identification Method Based on Multispectral Remote Sensing. Procedia Environ Sci 11, 1482–1487. https://doi.org/10.1016/J.PROENV.2011.12.223.